

Stable spatiotemporal spinning solitons in a bimodal cubic-quintic medium

D. Mihalache,^{1,2} D. Mazilu,^{1,2} I. Towers,^{3,4} B. A. Malomed,³ and F. Lederer²

¹*Department of Theoretical Physics, Institute of Atomic Physics, P.O. Box MG-6, Bucharest, Romania*

²*Institute of Solid State Theory and Theoretical Optics, Friedrich-Schiller Universität Jena, Max-Wien-Platz 1, D-07743 Jena, Germany*

³*Department of Interdisciplinary Studies, Faculty of Engineering, Tel Aviv University, Tel Aviv 69978, Israel*

⁴*School of Mathematics and Statistics, Australian Defence Force Academy, Canberra ACT 2600, Australia*

(Received 12 November 2002; revised manuscript received 14 January 2003; published 14 May 2003)

We investigate the formation of stable spatiotemporal three-dimensional (3D) solitons (“light bullets”) with internal vorticity (“spin”) in a bimodal system described by coupled cubic-quintic nonlinear Schrödinger equations. Two relevant versions of the model, for the linear and circular polarizations, are considered. In the former case, an important ingredient of the model are four-wave-mixing terms, which give rise to a phase-sensitive nonlinear coupling between two polarization components. Thresholds for the formation of both spinning and nonspinning 3D solitons are found. Instability growth rates of perturbation eigenmodes with different azimuthal indices are calculated as functions of the solitons’ propagation constant. As a result, stability domains in the model’s parameter plane are identified for solitons with the values of the spins of their components $s=0$ and $s=1$, while all the solitons with $s \geq 2$ are unstable. The solitons with $s=1$ are stable only if their energy exceeds a certain critical value, so that, in typical cases, the stability region occupies $\approx 25\%$ of their existence domain. Direct simulations of the full system produce results that are in perfect agreement with the linear-stability analysis: stable 3D spinning solitons readily self-trap from initial Gaussian pulses with embedded vorticity, and easily heal themselves if strong perturbations are imposed, while unstable spinning solitons quickly split into a set of separating zero-spin fragments whose number is exactly equal to the azimuthal index of the strongest unstable perturbation eigenmode.

DOI: 10.1103/PhysRevE.67.056608

PACS number(s): 42.65.Tg

I. INTRODUCTION

Solitons, i.e., self-supporting localized pulses, are ubiquitous objects that occur in media of very different physical nature. Among various realizations that solitons find in physics, optical solitons may arguably be the most important one [1–3]. A new topic in theoretical and experimental studies of optical solitons are *spatiotemporal solitons* (STSs, alias “light bullets” [4], “superspikes” [5], or “multidimensional simltons,” in the case of a two-color solitons in quadratically nonlinear media [6]). These are completely localized traveling pulses of light in planar waveguides or bulk media, that feature self-localization in both the longitudinal and transverse directions. They are supported by simultaneous balance of diffraction and dispersion by nonlinear phase modulation. On one hand, STSs are physical objects of fundamental interest, as examples of stable self-sustained localized objects in two dimensions (2D) and, especially, in three-dimensional (3D) nonlinear media are rare in physics. On the other hand, STSs (first of all, their 2D species) hold promise for potential applications to ultrafast all-optical processing devices, where each STS may represent an elementary bit of information, provided that *stable* STSs can be formed from pulses at reasonable energy levels in available optical materials [7].

As well as spatial and temporal solitons, STSs can be supported by nonlinearities of different types. However, being 2D or 3D objects, they may be subject to instability due to the possibility of wave collapse in multidimensional media. In particular, the ubiquitous cubic (Kerr) nonlinearity gives rise to collapse in both 2D and 3D cases [8,9], which makes the existence of stable STSs in uniform media with

the pure cubic nonlinearity impossible. Stability of STSs can be achieved in the case of saturable [5,10,11] or quadratic [$\chi^{(2)}$] [12–15] nonlinearity, as well as in graded-index Kerr media [16] and in engineered “tandem” structures built of quadratically nonlinear slices periodically alternating with linear layers [17]. The STS can also form in off-resonance two-level systems [18] and in media exhibiting self-induced transparency [19]. While the majority of works on STSs were dealing with solitons of the bright type, dark STSs were considered too [20].

Parallel to the theoretical activity, progress has been recently made in experimental studies. For the first time, a 2D STS was observed in a $\chi^{(2)}$ optical crystal [21]. These experiments employed the technique of achromatic phase-matching or tilted-pulse wave fronts, that was used earlier in the first experimental observation of temporal solitons in quadratically nonlinear crystals [22]. As the size of the available $\chi^{(2)}$ crystals is a few centimeters, reliable observation of STSs is possible if their dispersion and diffraction lengths z_{diff} and z_{disp} (which should be of the same order of magnitude, as both dispersion and diffraction are to be simultaneously balanced by the nonlinearity), are $\lesssim 1$ cm [21]. In the usual paraxial approximation, the diffraction length is estimated as $z_{\text{diff}} \sim k(\Delta x)^2$, where $k \equiv 2\pi/\lambda$ is the carrier wave number, λ is the corresponding wavelength, and Δx is the transverse size of the STS and of the initial pulse from which it may self-trap (see below). As the carrier wavelength is $\lesssim 1 \mu\text{m}$, this implies a constraint $\Delta x \lesssim 30 \mu\text{m}$ (which is still sufficiently large in comparison with the underlying wavelength, hence the paraxial approximation applies). The dispersion length is estimated as $z_{\text{disp}} \sim D(\Delta t)^2$, where D is the group-velocity-dispersion coefficient and Δt is the tem-

poral width of the pulse. Assuming that Δt cannot be essentially smaller than 100 fs, the constraint $z_{\text{disp}} \leq 1$ cm implies a necessary size of the dispersion coefficient $D \sim 1$ m/ps². As a matter of fact, these estimates apply not only to χ^2 crystals, but also to all materials in which STS may be created. A great challenge for the experimentalist is direct observation of a fully localized 3D STS under these conditions.

In addition to nonspinning solitons (that is, solitons with zero topological charge), spinning (vortex) solitons are also possible in a variety of optical media. Starting with the seminal works of Ref. [23], both delocalized (“dark”) and localized (“bright”) optical vortices in various 2D settings were investigated [24–29]. In the 3D case, spinning solitons take the shape of a torus (“doughnut”) [30,31]. For bright vortex solitons, stability is a major issue as, unlike their zero-spin counterparts, the spinning solitons are prone to destabilization by azimuthal perturbations. In the 2D case with $\chi^{(2)}$ and saturable nonlinearities, the azimuthal instability was revealed by simulations [25,26] and observed experimentally [27]. As a result, a soliton with spin 1 splits into two or three fragments, each being a moving stable zero-spin soliton. Numerical simulations of the 3D spinning STS in the pure $\chi^{(2)}$ model also demonstrate its instability-induced splitting into separating zero-spin solitons [31].

Nevertheless, the quadratic nonlinearity acting in combination with the self-defocusing cubic nonlinearity [32,33] give rise to stable spinning 2D solitons (alias ring vortices) with spins $s = 1$ and 2 [34], and to stable spinning doughnut-shaped 3D solitons with $s = 1$ [35]. All the 2D solitons with $s \geq 3$ and 3D solitons with $s \geq 2$ are unstable. Similar 2D and 3D spinning solitons may also be stable in another model, based on competing self-focusing cubic and self-defocusing quintic nonlinearities [36–38]. Optical nonlinearities of this *cubic-quintic* (CQ) type has been recently reported in chalcogenide glasses [39] and in organic materials [40].

In the first simulations of 2D solitons with $s = 1$ in the CQ model, it was found that they are robust, provided that their power is not too small [41]. Later analysis, based on the computation of linear-stability eigenvalues, has demonstrated that some of the 2D spinning solitons considered in Ref. [41] are subject to a weak azimuthal instability. Nonetheless, in another part of their existence region, with still larger powers, the solitons with $s = 1$ and $s = 2$ were confirmed to be stable in the *scalar* (single-component) 2D CQ model [36] (concerning the stability of solitons with $s = 1$, see also Ref. [42]).

Spinning 2D solitons were also considered in a *bimodal* (two component, also known as vectorial) model based on two nonlinearly coupled nonlinear Schrödinger (NLS) equations, which take into regard two orthogonal polarizations of light. If the nonlinearity is saturable, and the nonlinear coupling is of the cross-phase-modulation (XPM) type, two-component solitons remain unstable against azimuthal perturbations, although it was demonstrated that the instability of the soliton with opposite values of the spins in its two components, $s_1 = -s_2$, may be essentially weaker than that of the soliton with $s_1 = s_2$ [43] (two-component solitons with different vorticities in its components were also considered in Ref. [29]). On the other hand, the recent work [44] has

demonstrated that a two-component model of the CQ type gives rise to stable 2D spinning solitons (a multidimensional bimodal CQ model was first introduced in Ref. [45]; it shares some features with a model of light propagation in a CQ nonlinear medium equipped with a Bragg grating, where the two components represent right- and left-traveling waves, resonantly coupled by the Bragg reflection [46]). The cubic part of that model includes not only the XPM coupling, but also the four-wave-mixing (FWM) term, which is a coherent (phase-sensitive) nonlinear coupling between the two fields. In the presence of the FWM terms, the vectorial spinning solitons may only exist with equal values of the spins in its two components, $s_1 = s_2$. Stable 2D vortex solitons in both the scalar and vectorial CQ models are readily generated by initial Gaussian pulses with embedded vorticity [44,47].

As it was mentioned above, in the 3D case, stable bright spinning STSs with $s = 1$ have been recently identified in both the scalar CQ models [38] and in one combining the quadratic and self-defocusing cubic nonlinearities [35]. It is relevant to stress that the only previously known physical model that supports stable 3D vortex solitons was the famous field-theory Skyrme model [48], in which the spinning solitons represent nucleons (this model has recently found a new application to two-component Bose-Einstein condensation [49]). In both the CQ and quadratic-cubic models, the spinning 3D solitons are stable provided that they are sufficiently broad (i.e., their energy exceeds a certain threshold value), otherwise they are subject to the usual azimuthal instability [50].

At present, the study of the formation of complex soliton structures, such as clusters of several 2D or 3D solitons is also of much interest [51]. Such complex structures might be of importance for potential applications in future digital-imaging processing devices based on soliton light spots. Soliton clusters can be viewed as a nontrivial generalization of “spinning” solitons (or doughnutlike vortices) and necklace-ring beams [52,53], and they also appear in the study of active nonlinear systems such as driven optical cavities [54].

An issue of obvious interest is a generalization of the 3D spinning solitons to the case of a bimodal system including two polarizations of light, similar to the above-mentioned 2D model [44]. The aim of the present work is to construct bimodal bright 3D spinning solitons in the vectorial CQ model (including FWM terms) and to investigate their stability. In this work, we consider the vectorial CQ model in two generic situations: (i) for two linear polarizations, when the relative cubic-XPM coefficient is $\alpha = 2/3$, and (ii) two circular polarizations, when $\alpha = 2$.

An inherent ingredient of any model based on the linear polarizations is the FWM term [1]. In the case of the long-distance propagation in optical fibers, the FWM term is usually dropped because it effectively averages to zero due to rapid phase oscillations induced by the fiber’s birefringence [1]. However, experiments with spatial (see, e.g., Ref. [55]) and spatiotemporal [21] solitons imply a short propagation distance, which may be smaller than the birefringence beat length, hence the FWM terms must be kept in the model (as it was done in the 2D case [44]). As it was mentioned above,

the FWM terms admit only bimodal spinning soliton with identical values of the vorticity in both components. Generally, the effect of the FWM-induced *coherent* nonlinear coupling between the components on the stability of bimodal solitons is quite an interesting issue by itself.

The model with $\alpha=2$, valid for circular polarizations, does not include FWM terms. In fact, this version of the model applies not only to the case of two circular polarizations, but also to copropagation of two waves with different carrier wavelengths [1].

The rest of the paper is organized as follows. In Sec. II, the vectorial CQ model is formulated, and general results concerning the existence of 3D spinning solitons in it are displayed. Fundamental results for stability of the spinning solitons, based on eigenvalues found from equations linearized around the stationary soliton solutions, are presented in Sec. III. Direct numerical simulations of the stability of the spinning solitons are presented in Sec. IV. The results of the work are summarized in the concluding section.

II. THE VECTORIAL CUBIC-QUINTIC MODEL AND STATIONARY SOLUTIONS FOR 3D SPINNING SOLITONS

We consider a bimodal system described by two nonlinearly coupled NLS equations that incorporate the self-defocusing quintic nonlinearity. A general form of the corresponding CQ system was introduced in Ref. [45]. To recapitulate the derivation, we assume that the physical (real) electric field is a combination of two polarizations with complex amplitudes \mathcal{E}_1 and \mathcal{E}_2 , oriented along mutually orthogonal transverse unit vectors $\mathbf{e}_{1,2}$:

$$\mathbf{E} = \mathcal{E}_1 e^{i\phi_1} \mathbf{e}_1 + \mathcal{E}_2 e^{i\phi_2} \mathbf{e}_2 + \text{c.c.}, \quad (1)$$

where c.c. stands for the complex-conjugate expression, $\phi_{1,2} = -\omega t + (k \pm \frac{1}{2} \Delta k) z$ are rapidly varying phases of the two waves with common carrier frequency ω and mean wave number k (t and z are time and propagation coordinates), and the small shifts $\pm \Delta k/2$ accounting for linear phase-velocity birefringence. In the most relevant case of the isotropic nonlinearity, the self-focusing cubic and self-defocusing quintic nonlinear corrections to the refractive index are proportional, respectively, to

$$\mathbf{E}^2 \equiv (\mathcal{E}_1^2 e^{2i\phi_1} + \mathcal{E}_2^2 e^{2i\phi_2}) + \text{c.c.} + 2(|\mathcal{E}_1|^2 + |\mathcal{E}_2|^2) \quad (2)$$

and $(\mathbf{E}^2)^2$.

Following the lines of the standard derivation of the corresponding system of coupled NLS equations [1] and using the expression (2) and its square, we arrive at the system of equations that are valid under the usual paraxial and slowly varying envelope-amplitude approximations:

$$\begin{aligned} i \frac{\partial u}{\partial Z} + \left(\frac{\partial^2 u}{\partial X^2} + \frac{\partial^2 u}{\partial Y^2} + \frac{\partial^2 u}{\partial T^2} \right) + \beta u + \chi^{(3)} \left[\left(|u|^2 + \frac{2}{3} |v|^2 \right) u \right. \\ \left. + \frac{1}{3} v^2 u^* \right] - \chi^{(5)} \left[\left(|u|^4 + \frac{6}{5} |u|^2 |v|^2 + \frac{3}{5} |v|^4 \right) u \right. \\ \left. + \frac{1}{5} (3|u|^2 + 2|v|^2) v^2 u^* + \frac{1}{5} e^{2i\beta Z} u^3 (v^*)^2 \right] = 0, \quad (3) \end{aligned}$$

$$\begin{aligned} i \frac{\partial v}{\partial Z} + \left(\frac{\partial^2 v}{\partial X^2} + \frac{\partial^2 v}{\partial Y^2} + \frac{\partial^2 v}{\partial T^2} \right) - \beta v + \chi^{(3)} \left[\left(|v|^2 + \frac{2}{3} |u|^2 \right) v \right. \\ \left. + \frac{1}{3} u^2 v^* \right] - \chi^{(5)} \left[\left(|v|^4 + \frac{6}{5} |v|^2 |u|^2 + \frac{3}{5} |u|^4 \right) v \right. \\ \left. + \frac{1}{5} (3|v|^2 + 2|u|^2) u^2 v^* + \frac{1}{5} e^{-2i\beta Z} v^3 (u^*)^2 \right] = 0. \quad (4) \end{aligned}$$

Here, $u \sim \mathcal{E}_1$ and $v \sim \mathcal{E}_2$ are properly normalized amplitudes of the two modes, the asterisk stands for the complex conjugation, $\chi^{(3)}$ and $\chi^{(5)}$ are effective coefficients of the cubic and quintic nonlinearities, $\beta \sim \Delta k$ is a normalized birefringence parameter, Z and X, Y are normalized propagation and transverse spatial coordinates, and T is the normalized temporal variable in the reference frame of the carrier wave.

Similarly, if the field is composed of circular modes \mathcal{E}_\pm aligned with transverse vectors $\mathbf{e}_\pm = (\mathbf{e}_1 \pm i\mathbf{e}_2)/\sqrt{2}$, which are subject to relations $\mathbf{e}_1^2 = \mathbf{e}_2^2 = 0$ and $\mathbf{e}_1 \cdot \mathbf{e}_2 = 1$, so that $\mathbf{E} = \mathcal{E}_+ e^{i\phi_+} \mathbf{e}_+ + \mathcal{E}_- e^{i\phi_-} \mathbf{e}_- + \text{c.c.}$ and

$$\mathbf{E}^2 = 2[\mathcal{E}_+ \mathcal{E}_- e^{i(\phi_+ + \phi_-)} + \text{c.c.}] + 2(|\mathcal{E}_+|^2 + |\mathcal{E}_-|^2). \quad (5)$$

Again assuming isotropy of the cubic and quintic nonlinearities, straightforward analysis using expression (5) and its square leads to the following coupled equations which, unlike Eqs. (3) and (4), do not contain FWM terms:

$$\begin{aligned} i \frac{\partial u}{\partial Z} + \left(\frac{\partial^2 u}{\partial X^2} + \frac{\partial^2 u}{\partial Y^2} + \frac{\partial^2 u}{\partial T^2} \right) + \beta u + \chi^{(3)} (|u|^2 + 2|v|^2) u \\ - \chi^{(5)} (|u|^4 + 6|u|^2 |v|^2 + 3|v|^4) u = 0, \quad (6) \end{aligned}$$

$$\begin{aligned} i \frac{\partial v}{\partial Z} + \left(\frac{\partial^2 v}{\partial X^2} + \frac{\partial^2 v}{\partial Y^2} + \frac{\partial^2 v}{\partial T^2} \right) - \beta v + \chi^{(3)} (|v|^2 + 2|u|^2) v \\ - \chi^{(5)} (|v|^4 + 6|v|^2 |u|^2 + 3|u|^4) v = 0, \quad (7) \end{aligned}$$

where, this time, u and v are properly normalized amplitudes \mathcal{E}_\pm .

Our simulations have demonstrated that quintic XPM terms in Eq. (3) through Eq. (7), as well as quintic FWM terms in Eqs. (3) and (4), do not affect stability of spin-carrying STSs in any conspicuous way [particularly, the last FWM terms in the latter equations are negligible due to both the small numerical factor 1/5 and oscillating factors $\exp(\pm 2i\beta z)$]. On the other hand, the influence of the cubic XPM and FWM terms was found to be more essential. For this reason, and aiming to present results in a sufficiently compact form, we adopt the following simplified but adequate model, which includes SPM, XPM, and FWM cubic terms, and only SPM quintic ones:

$$iu_Z + u_{XX} + u_{YY} + u_{TT} + \beta u + (|u|^2 + \alpha|v|^2)u + \gamma v^2 u^* - |u|^4 u = 0, \quad (8)$$

$$iv_Z + v_{XX} + v_{YY} + v_{TT} - \beta v + (|v|^2 + \alpha|u|^2)v + \gamma u^2 v^* - |v|^4 v = 0. \quad (9)$$

We will consider two specific versions of the system, viz., with $\alpha=2/3$ and $\gamma=1/3$ for the case of two orthogonal linear polarizations and with $\alpha=2$ and $\gamma=0$ for the case of two circular polarizations. Thus, in either case, we are left with the single control parameter β in Eqs. (8) and (9).

Stationary solutions to Eqs. (8) and (9) are sought for in the forms $u = U(r, T) \exp(i\kappa Z + is\theta)$ and $v = V(r, T) \exp(i\kappa Z + is\theta)$, where r and θ is the polar coordinates in the plane (X, Y) , κ are the wave number shift, and the integer s is the spin (recall that the presence of the FWM terms dictates the choice of identical vorticities in both components). The functions U and V may be taken real, obeying equations

$$\frac{\partial^2 U}{\partial r^2} + \frac{1}{r} \frac{\partial U}{\partial r} + \frac{\partial^2 U}{\partial T^2} - \frac{s^2}{r^2} U + (\beta - \kappa)U + (U^2 + \alpha V^2)U - U^5 + \gamma V^2 U = 0,$$

$$\frac{\partial^2 V}{\partial r^2} + \frac{1}{r} \frac{\partial V}{\partial r} + \frac{\partial^2 V}{\partial T^2} - \frac{s^2}{r^2} V + (-\beta - \kappa)V + (\alpha U^2 + V^2)V - V^5 + \gamma U^2 V = 0, \quad (10)$$

following from Eqs. (8) and (9).

Equations (8) and (9) conserve the net energy (which is proportional to the number of photons trapped in the field),

$$E = \int \int \int (|u|^2 + |v|^2) dX dY dT \equiv E_u + E_v, \quad (11)$$

the Hamiltonian

$$H = \int \int \int \left\{ |u_X|^2 + |u_Y|^2 + |u_T|^2 + |v_X|^2 + |v_Y|^2 + |v_T|^2 - \beta|u|^2 + \beta|v|^2 - \frac{1}{2} \gamma (u^* v^2 + u^2 v^*) \right. \\ \left. + \left[-\frac{1}{2} (|u|^4 + 2\alpha|u|^2|v|^2 + |v|^4) + \frac{1}{3} (|u|^6 + |v|^6) \right] \right\} dX dY dT, \quad (12)$$

momentum (equal to zero for the solutions considered), and angular momentum in the transverse plane [2].

We have numerically found one-parameter families of stationary 3D spinning solitons, which have the shape of vortex tori with a hole (supported by a phase dislocation) in the center. A standard band-matrix numerical algorithm was used to deal with the corresponding two-point boundary-value problem based on Eqs. (10). According to results of previous

works [34–36,38], it is very likely that the solitons with $s > 2$ are unstable, therefore we concentrated on the study of the stability of the spinning solitons with $s = 1$ and 2. In fact, it was found that, as well as in the corresponding 3D scalar model (see Ref. [38]) and in its quadratic-cubic counterpart [35], only the spinning STS with $s = 1$ may be stable (provided that its energy is sufficiently large).

As well as in the scalar CQ model [30,38], the existence region of the two-component (vectorial) 3D spinning solitons is limited by maximum wave number shift κ_{offset} , such that at $\kappa = \kappa_{\text{offset}}$ the outer size of STS diverges, but the size of its internal hole remains finite. This means that at $\kappa = \kappa_{\text{offset}}$, the $s=0$ soliton goes over into a uniform continuous-wave state, while bright solitons with $s \geq 1$ turn over into a cylindrical dark soliton. However, an important difference from the single-component model is that, in the vectorial one including the FWM terms, κ_{offset} depends on the birefringence parameter β .

In Fig. 1, we summarize outputs of extensive numerical calculations aimed at detecting domains of existence and linear stability of the spinning solitons in the vectorial CQ model including the FWM terms [the one with $\alpha=2/3$ and $\gamma=1/3$ in Eqs. (8) and (9); details of the stability analysis are given below]. The domains are presented in a comprehensive form in the parametric plane (κ, β) . The upper continuous curve is the line $\kappa_{\text{offset}}(\beta)$, which is the common existence border of all the bright solitons irrespective of the value of s , while the lower continuous curve and the dash-dotted one near it are lower borders of the existence domain of the solitons for different values of s . The two dashed lines in Fig. 1 mark the lower stability boundaries for the solitons with $s = 0$ and 1. Thus, the zero-spin solitons are stable in a larger part of their existence domain, while the spinning solitons with $s = 1$ are stable in a relatively narrow (in terms of κ) region abutting on the upper existence border; particularly, the $s=1$ solitons are stable for $\kappa > 0.5$ if $\beta=0$. In these stability regions, the solitons are broad [“heavy,” with large values of their energy (11), see Figs. 2 and 3].

In Figs. 2 and 3, we plot the curves $\kappa = \kappa(E)$ and $H = H(E)$ corresponding to the families of the zero-spin and spinning STSs for the model with $\alpha=2/3$ and $\gamma=1/3$. To display the results, we have selected two representative values of the birefringence parameter, $\beta=0$ and $\beta=0.2$. For the sake of comparison, we also plot the corresponding curves for the single-component (scalar) STSs (the ones with $v \equiv 0$, that we call *simple solitons*). Obviously, they are particular solutions of the present model.

We see that the vectorial STSs (alias *composite solitons*) bifurcate from the corresponding simple ones at certain values of κ . Note that the composite solitons appear as unstable solutions, and (in the case $s=0$ and $s=1$) they get stabilized at larger values of κ . An essential feature of all the 3D solitons, which is evident in Figs. 2 and 3, is the presence of a finite minimum energy (threshold) necessary for their existence, the threshold values increasing with s . The full and dashed lines in Figs. 2 and 3 correspond to solutions that are stable and unstable, respectively, against small perturbations, according to results presented below. In particular, the stabil-

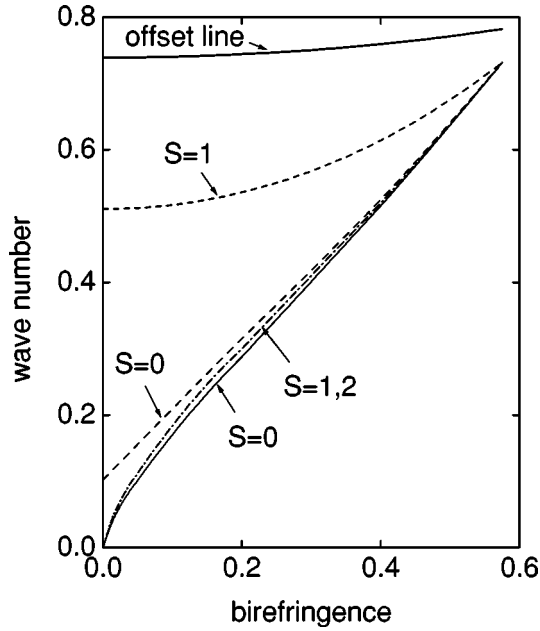


FIG. 1. Domains of existence and stability of two-component solitons with the values of the spins $s=0, 1$, and 2 of their components. The lower and upper continuous curves and the lower dash-dotted one border the existence regions. The two dashed lines mark the stability domains; see further explanations in the text. This figure and the ones displayed below, except for Figs. 4 and 7, pertain to the model with the linear polarizations ($\alpha=2/3$ and $\gamma=1/3$).

ity of the $s=0$ solitons completely agrees with the known Vakhitov-Kolokolov criterion, which states that the fundamental ($s=0$) soliton branch may only undergo a stability change at a point where $dE/d\kappa$ vanishes [56]. Global stability of the solitons may be estimated by their “chemical potential,” i.e., the ratio of the Hamiltonian to the energy (number of photons). As is obvious from Figs. 2(b) and 3(b), this ratio always takes a smaller (more negative) value for the composite solitons, hence they are expected to be more stable in the global sense, according to the well-known principle stating that the system prefers to minimize its Hamiltonian for a fixed value of the energy (number of photons) [9].

In Fig. 4, plotted are the curves $\kappa=\kappa(E)$ and $H=H(E)$ pertaining to the zero-spin and spinning STSs in the other version of the model, with $\alpha=2$ and $\gamma=0$ (which corresponds to the circular polarizations). From the comparison of this figure and Fig. 2, we conclude that there is no qualitative difference between both versions of the model.

III. STABILITY OF THE THREE-DIMENSIONAL SPINNING SOLITONS

The most revealing information on the stability of solitons is provided by the analysis of Eqs. (8) and (9) linearized about the stationary solution. To this end, we seek for perturbation eigenmodes in a general form

$$\begin{aligned} u(Z, r, T, \theta) - U(r, T) \exp[i(s\theta + \kappa Z)] \\ = f(r, T) \exp\{\lambda_n Z + i[(s+n)\theta + \kappa Z]\} + g^*(r, T) \\ \times \exp\{\lambda_n^* Z + i[(s-n)\theta + \kappa Z]\}, \end{aligned} \quad (13)$$

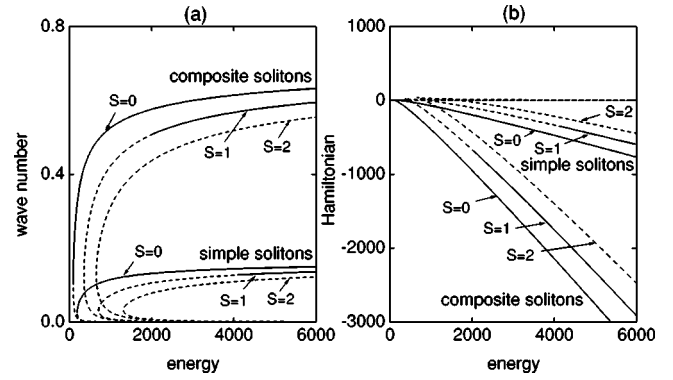


FIG. 2. The wave number κ (a) and Hamiltonian H (b) of the three-dimensional two-component solitons, with different values of the spins of their components, vs the soliton’s energy E , for $\beta=0$.

$$\begin{aligned} v(Z, r, T, \theta) - V(r, T) \exp[i(s\theta + \kappa Z)] \\ = p(r, T) \exp\{\lambda_n Z + i[(s+n)\theta + \kappa Z]\} + q^*(r, T) \\ \times \exp\{\lambda_n^* Z + i[(s-n)\theta + \kappa Z]\}, \end{aligned} \quad (14)$$

where $n>0$ is an arbitrary integer azimuthal index of the perturbation and λ_n is the (complex) eigenvalue that should be found. This form of the infinitesimal perturbation is a closed one (no other values of the perturbation azimuthal index but n and $s-n$ are generated). The functions f, g and p, q which appear in Eqs. (13) and (14) obey the following equations:

$$\begin{aligned} i\lambda_n f + \frac{d^2 f}{dr^2} + r^{-1} \frac{df}{dr} + \frac{d^2 f}{dT^2} - (s+n)^2 r^{-2} f + (\beta - \kappa) f \\ + (2U^2 + \alpha V^2 - 3U^4) f + (U^2 + \gamma V^2 - 2U^4) g \\ + (\alpha + 2\gamma) UV p + \alpha UV q = 0, \end{aligned} \quad (15)$$

$$\begin{aligned} -i\lambda_n g + \frac{d^2 g}{dr^2} + r^{-1} \frac{dg}{dr} + \frac{d^2 g}{dT^2} - (s-n)^2 r^{-2} g + (\beta - \kappa) g \\ + (2U^2 + \alpha V^2 - 3U^4) g + (U^2 + \gamma V^2 - 2U^4) f \\ + (\alpha + 2\gamma) UV q + \alpha UV p = 0, \end{aligned} \quad (16)$$

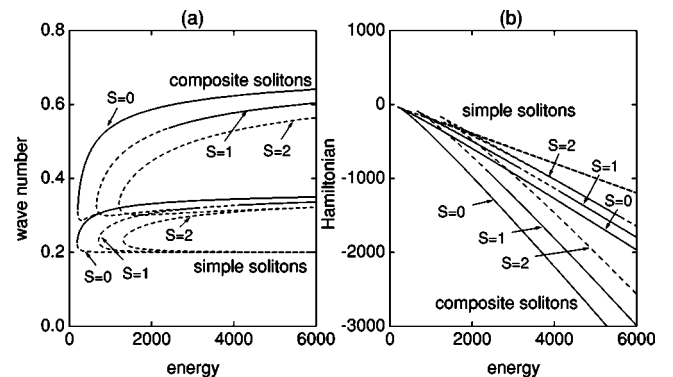


FIG. 3. The same as in Fig. 2, but for $\beta=0.2$.

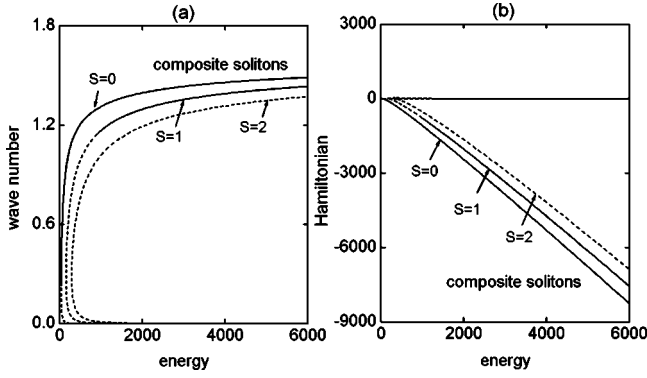


FIG. 4. The same as in Fig. 2, but for the model with two circular polarizations ($\alpha=2$ and $\gamma=0$).

$$\begin{aligned}
 & i\lambda_n p + \frac{d^2 p}{dr^2} + r^{-1} \frac{dp}{dr} + \frac{d^2 p}{dT^2} - (s+n)^2 r^{-2} p + (-\beta - \kappa) p \\
 & + (\alpha U^2 + 2V^2 - 3V^4) p + (\gamma U^2 + V^2 - 2V^4) q \\
 & + (\alpha + 2\gamma) UVf + \alpha UVg = 0,
 \end{aligned} \tag{17}$$

$$\begin{aligned}
 & -i\lambda_n q + \frac{d^2 q}{dr^2} + r^{-1} \frac{dq}{dr} + \frac{d^2 q}{dT^2} - (s-n)^2 r^{-2} q + (-\beta - \kappa) q \\
 & + (\alpha U^2 + 2V^2 - 3V^4) q + (\gamma U^2 + V^2 - 2V^4) p \\
 & + (\alpha + 2\gamma) UVg + \alpha UVf = 0.
 \end{aligned} \tag{18}$$

The solutions of these equations must decay exponentially at $r \rightarrow \infty$ and $T \rightarrow \infty$. At $r \rightarrow 0$, f and p must vanish as $r^{|s+n|}$, whereas g and q vanish as $r^{|s-n|}$.

To solve Eq. (15) through Eq. (18) and to find the eigenvalues, we used a known numerical procedure [25,26,57], which has produced results presented in Fig. 5. The most persistent unstable eigenmode has $n=2$, for both $s=1$ and $s=2$. As is seen in Fig. 5(a), the instability of the soliton with $s=1$, accounted for by $\text{Re } \lambda(n=2)$ disappears with the increase of κ at a stability-change point $\kappa_{st} \approx 0.54$, and the stability region extends up to $\kappa = \kappa_{\text{offset}} \approx 0.74$, corresponding to the upper continuous line in Fig. 1, i.e., up to infinitely broad solitons with infinite energy, as it was explained

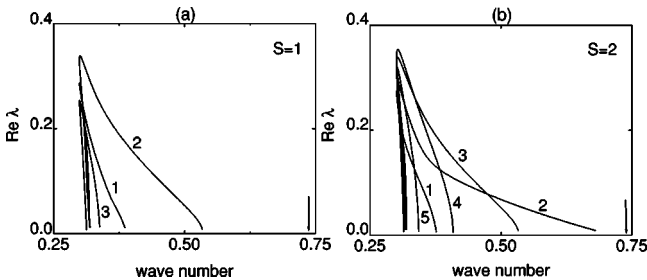


FIG. 5. The instability growth rate, $\text{Re } \lambda$, of the perturbation eigenmodes corresponding to different values of the azimuthal index n (the value is attached to each curve) vs the soliton's wave-number κ : (a) $s=1$; (b) $s=2$. Here $\beta=0.2$. The point at which the size of the solitons diverges (the border of their existence region) is marked by the vertical arrow.

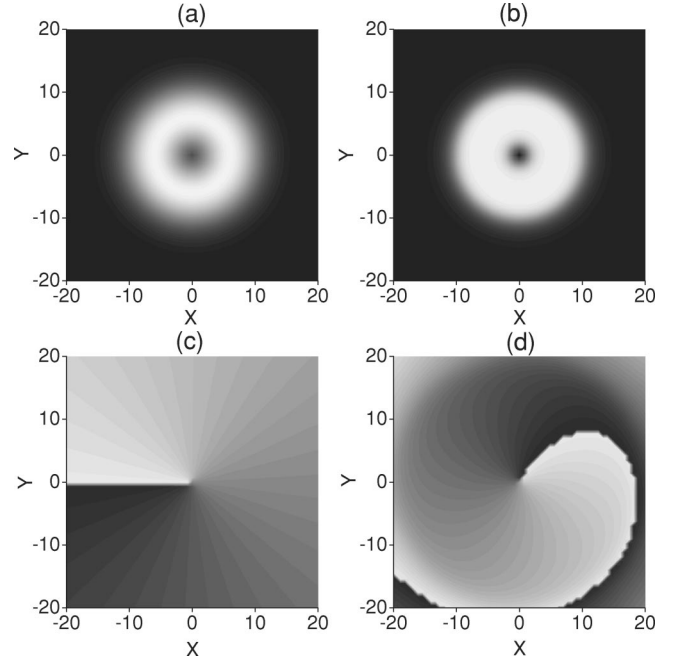


FIG. 6. Formation of the two-component soliton with $s=1$ from a Gaussian input with a trapped vortex and initial energy $E = 6670$ in the case $\beta=0.2$. Shown are the gray-scale plots of the u field: the intensity distribution in the initial (a) (at $Z=0$) and final (b) (at $Z=200$) pulses, and the corresponding phase fields (c) and (d). The v field undergoes similar evolution.

above. This result implies that a vectorial (two-component) optical vortex of the dark-soliton type, that may be regarded as an infinitely broad $s=1$ spinning dark cylindrical soliton of the present type, is stable too.

For the birefringence taking values in the interval $0 < \beta < 0.2$, the relative width of the stability region of the bright solitons with $s=1$ is $(\kappa_{\text{offset}} - \kappa_{st}) / \kappa_{\text{offset}} \approx 25\%$ [see Figs. 1 and 5(a)]. It is slightly larger than the relative size of the soliton stability region that was found in the scalar counterpart of the model [38]. No stability region exists for the solitons with $s=2$ [see Fig. 5(b)], in full accordance with what had been found earlier for the 3D spatiotemporal spinning solitons with $s=2$ in both the CQ and quadratic-cubic [35] scalar models.

In the case when the spinning solitons considered here are unstable, their instability is *oscillatory* [58]. The corresponding frequency $\text{Im } \lambda$ (which is not shown in Fig. 5) is of the same order of magnitude as $\text{Re } \lambda$ at the maximum-instability point, and λ is purely imaginary at $\kappa \geq \kappa_{st}$. This feature is also similar to what is known about the solitons in the scalar CQ model [38].

IV. DIRECT NUMERICAL SIMULATIONS

It is necessary to check how the above results for the stability, based on the calculation of eigenvalues from the linearized equations, match to direct simulations of the full nonlinear Eqs. (8) and (9). To this end, the simulations were carried out by dint of the standard Crank-Nicholson scheme, which implies solving the equations by means of the Picard

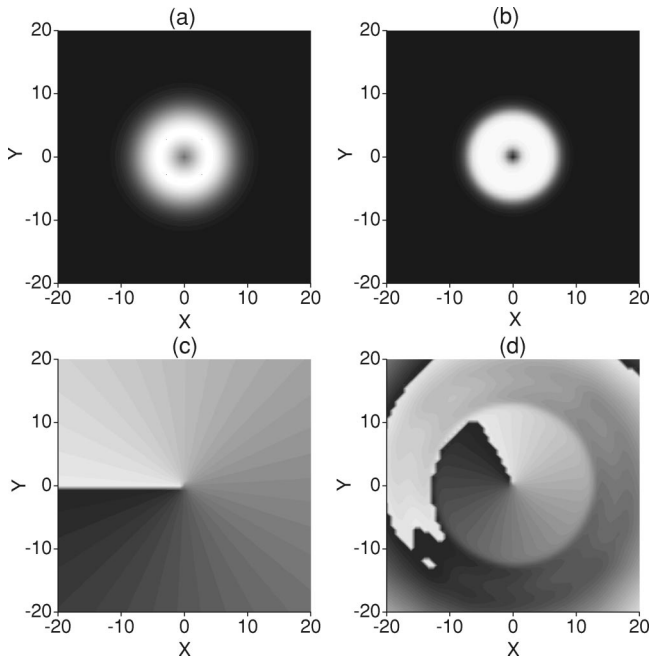


FIG. 7. The same as in Fig. 6, but for the model with circular polarizations ($\alpha=2$ and $\gamma=0$), the initial energy of the Gaussian pulse with the trapped vorticity being $E=4110$.

iteration method [59], the resulting linear system being handled by means of the Gauss-Seidel iterative scheme. To achieve good convergence, we needed, typically, ten Picard iterations and four Gauss-Seidel iterations. In most cases, we employed the transverse-grid's stepsize $\Delta X = \Delta Y = \Delta T = 0.2$, and the longitudinal step size $\Delta Z = 0.02$. To avoid distortion of the instability development under the action of very small perturbations introduced by the Cartesian computational mesh, we explicitly added larger random perturbations to the initial state, cf. simulations of the stability of zero-spin solitons performed in the model with saturable nonlinearity in Ref. [11].

To test the robustness of the sufficiently broad (heavy) spinning solitons with $s=1$, which were found above to be stable against small perturbations in the model with $\alpha=2/3$ and $\gamma=1/3$ (corresponding to two linear polarizations), we simulated self-trapping of a soliton from an initial Gaussian pulse with the energy $E_0=6670$ [see Eq. (11)], onto which a

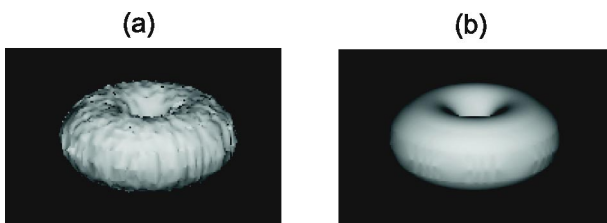


FIG. 8. The recovery of the stationary soliton with $s=1$, which was perturbed by strong random noise at $Z=0$: (a) the intensity distribution in the initial perturbed soliton; (b) the same in the self-cleared one at $Z=100$. The parameters are $\kappa=0.55$ and $\beta=0.2$. The numerical simulations were performed in the box $[-21,21] \times [-21,21] \times [-21,21]$.

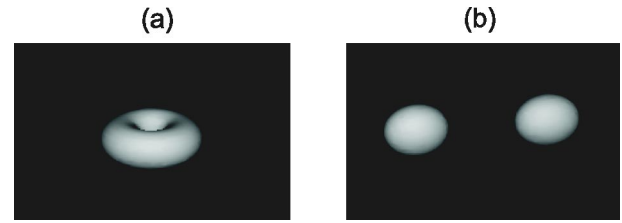


FIG. 9. Isosurface plots illustrating the evolution of the unstable soliton with $s=1$, $\kappa=0.4$, and $\beta=0.2$. (a) $Z=0$; (b) $Z=60$. The numerical simulations were performed in the same box as in Fig. 8.

phase dislocation with $s=1$ was superimposed. Figure 6 shows gray-scale plots of the distribution of the intensity and phase of the u field in the transverse (x,y) plane, for both the input Gaussian with the trapped vortex (at $Z=0$) and the emerging spinning soliton with $s=1$ at $Z=200$. The v field, which is not displayed here, shows similar behavior.

In Fig. 7, we show the formation of a stable spinning soliton with $s=1$ in the other version of the model, with $\alpha=2$ and $\gamma=0$, corresponding to two circular polarizations. Here the energy of the input Gaussian with the embedded vorticity is $E_0=4110$. As before, the behavior of the v component is similar to that of the u component, which is displayed in Fig. 7.

Thus, the robustness of the 3D STSs (vortex tori) is attested to by the fact, obvious from Figs. 6 and 7, that they can be generated from initial Gaussian pulses with the trapped vortex, whose shape is far from the exact form of the soliton. We conclude from Figs. 6 and 7 that the input Gaussian reshapes itself, which leads to redistribution of the net energy between the two components; some energy loss occurs, which is caused by emission of radiation in the course of the formation of the stable spinning soliton.

One might assume that, very generally speaking, the vorticity-carrying soliton is not an absolutely stable object, but rather a metastable one. Indeed, it is suggested by Figs. 2(a), 3(a), and 4(a) that the value of the Hamiltonian of the spinning STS is, generally, *larger* than that of its zero-spin counterpart containing the same number of photons, hence one may be wondering if a very strong initial perturbation could provoke rearrangement of the spinning soliton into a zero-spin one, the angular momentum being carried away with emitted radiation. An implication of this question is that the stability of the 3D spinning STSs with $s=1$ against small perturbations is provided for by effective potential barriers

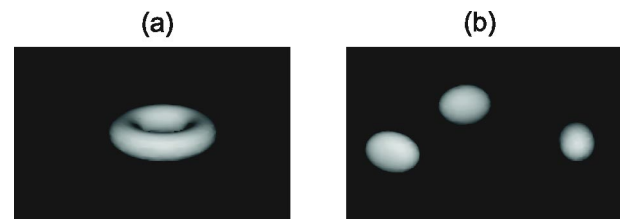


FIG. 10. Isosurface plots showing the fragmentation of the unstable soliton with $s=2$, $\kappa=0.44$, and $\beta=0.2$. (a) $Z=0$, (b) $Z=90$. The numerical simulations were performed in the box $[-30,30] \times [-30,30] \times [-30,30]$.

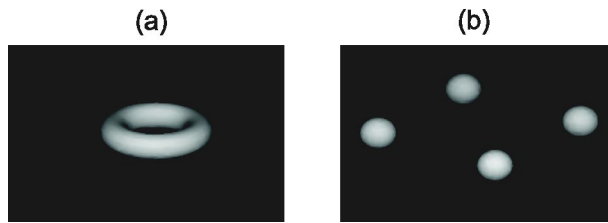


FIG. 11. The same as in Fig. 10, but for $\kappa=0.31$ and $\beta=0.2$. (a) $Z=0$; (b) $Z=50$. The numerical simulations were performed in the same box as in Fig. 10.

separating them from the solitons with $s=0$.

Further numerical results demonstrate that, in terms of this consideration, the spinning and nonspinning STSs are separated by extremely high barriers, which make the transition process $s \neq 0 \rightarrow s=0$ practically impossible. To illustrate this point, in Fig. 8, we display the intensity distributions inside a strongly perturbed initial soliton with $s=1$ (the amplitude of the random perturbation is $\approx 30\%$ of the soliton's amplitude), and in a finally established soliton. As it is obvious from Fig. 8, the soliton is able to completely heal the damage, remaining a truly stable object. In fact, a strong perturbation can transform the spinning STS into a zero-spin one only if the perturbation removes the soliton's vorticity.

In cases when the vectorial solitons with $s=1$ and $s=2$ are unstable against small perturbations, typical scenarios of the nonlinear instability development are illustrated by Figs. 9–11. The azimuthal instability eventually breaks the unstable spinning STS into a few stable zero-spin ones, which then fly out tangentially relative to the circular crest of the original soliton, quite similar to what is known about the instability-induced breakup of the scalar 2D vortex solitons [25,26,36,37], vectorial 2D vortex solitons [44], and scalar 3D spinning ones [38] in the CQ model. Thus, the initial internal angular momentum of the unstable torus-shaped vortex STS is converted into the orbital momentum of the emerging nonspinning fragments.

Analyzing results of many simulations, we have concluded that the number of the fragments is, roughly, twice the original spin s , and the dependence of the fragments' number on other parameters being fairly weak. We stress that results of direct simulations (particularly, those shown in Figs. 9–11) are in perfect agreement with the stability analysis based on the linearized equations: in all the cases, the number of the instability-generated fragments is *precisely* equal

to the azimuthal index of the perturbation eigenmode that has the largest instability growth rate (namely, $n=2,3$, and 4 in Figs. 9–11, respectively).

V. CONCLUSION

In this work, it has been shown that stable spatiotemporal solitons with intrinsic vorticity, that were recently found in the model of bulk media with nonlinear response combining self-focusing cubic and self-defocusing quintic terms, can also be found in a bimodal system that takes into regard two polarizations of light. Two basic versions of the bimodal system were considered, corresponding to linear and circular polarizations. The former one includes four-wave-mixing terms, hence two-component vortex solitons may only have equal values of spins s in both components, and the results depend, in a nontrivial way, on the birefringence parameter (the previously considered single-component model had no free parameters). Families of two-component spinning solitons were found to bifurcate from one-component solitons. Then, the vectorial solitons with the values of the spins $s=0$ and $s=1$ of their components become stable. Computation of eigenvalues shows that the stability region of the vectorial solitons with $s=1$ occupies approximately 25% of their existence domain, which is *larger* than in the case of scalar solitons. Another advantage of the vectorial solitons is that they have a smaller value of the Hamiltonian for the same energy (number of photons), i.e., they have a smaller value of the chemical potential, hence they are more stable than their single-component counterparts in the global sense. Direct simulations completely confirm predictions of the linear-stability analysis. In fact, the stable vectorial solitons with $s=1$ are strong *attractors*, as they readily self-trap from initial Gaussian pulses with embedded vorticity, and easily restore themselves after imposing strong perturbations. If the spinning solitons are unstable, they break up into separating zero-spin solitons whose number is exactly equal to the azimuthal index of the strongest unstable perturbation eigenmode.

ACKNOWLEDGMENTS

D. Mihalache and D. Mazilu acknowledge support from Deutsche Forschungsgemeinschaft (DFG). The work of I. T. was supported by Grant No. 1999459 from the U.S.-Israel Binational Science Foundation and by a matching grant from the Tel Aviv University.

-
- [1] G. P. Agrawal, *Nonlinear Fiber Optics* (Academic Press, San Diego, 1995).
 - [2] N. N. Akhmediev and A. Ankiewicz, *Solitons, Nonlinear Pulses and Beams* (Chapman and Hall, London, 1997).
 - [3] G.I. Stegeman, D.N. Christodoulides, and M. Segev, *IEEE J. Sel. Top. Quantum Electron.* **6**, 1419 (2000).
 - [4] Y. Silberberg, *Opt. Lett.* **15**, 1282 (1990).
 - [5] J.T. Manassah, P.L. Baldeck, and R.R. Alfano, *Opt. Lett.* **13**, 1090 (1988); J.T. Manassah, *ibid.* **16**, 563 (1991).
 - [6] H. He and P.D. Drummond, *Phys. Rev. E* **58**, 5025 (1998).
 - [7] R. McLeod, K. Wagner, and S. Blair, *Phys. Rev. A* **52**, 3254 (1995).
 - [8] B. Gross and J.T. Manassah, *Opt. Commun.* **129**, 143 (1996).
 - [9] L. Bergé, *Phys. Rep.* **303**, 260 (1998).
 - [10] N. Akhmediev and J.M. Soto-Crespo, *Phys. Rev. A* **47**, 1358 (1993).
 - [11] D.E. Edmundson, *Phys. Rev. E* **55**, 7636 (1997).
 - [12] A.A. Kanashov and A.M. Rubenchik, *Physica D* **4**, 122 (1981).
 - [13] K. Hayata and M. Koshiba, *Phys. Rev. Lett.* **71**, 3275 (1993); B.A. Malomed *et al.*, *Phys. Rev. E* **56**, 4725 (1997); D.V.

- Skryabin and W.J. Firth, *Opt. Commun.* **148**, 79 (1998); D. Mihalache, D. Mazilu, B.A. Malomed, and L. Torner, *ibid.* **152**, 365 (1998).
- [14] D. Mihalache, D. Mazilu, J. Döring, and L. Torner, *Opt. Commun.* **159**, 129 (1999).
- [15] D. Mihalache, D. Mazilu, B.A. Malomed, and L. Torner, *Opt. Commun.* **169**, 341 (1999); D. Mihalache, D. Mazilu, L.-C. Crasovan, L. Torner, B.A. Malomed, and F. Lederer, *Phys. Rev. E* **62**, 7340 (2000).
- [16] S. Raghavan and G.P. Agrawal, *Opt. Commun.* **180**, 377 (2000).
- [17] L. Torner, S. Carrasco, J.P. Torres, L.-C. Crasovan, and D. Mihalache, *Opt. Commun.* **199**, 277 (2001).
- [18] I.V. Mel'nikov, D. Mihalache, and N.-C. Panoui, *Opt. Commun.* **181**, 345 (2000).
- [19] M. Blaauboer, B.A. Malomed, and G. Kurizki, *Phys. Rev. Lett.* **84**, 1906 (2000).
- [20] Y. Chen and J. Atai, *Opt. Lett.* **20**, 133 (1995).
- [21] X. Liu, L.J. Qian, and F.W. Wise, *Phys. Rev. Lett.* **82**, 4631 (1999); X. Liu, K. Beckwitt, and F. Wise, *Phys. Rev. E* **62**, 1328 (2000).
- [22] P. Di Trapani, D. Caironi, G. Valiulis, A. Dubietis, R. Danielius, and A. Piskarskas, *Phys. Rev. Lett.* **81**, 570 (1998).
- [23] G.A. Swartzlander, Jr., and C.T. Law, *Phys. Rev. Lett.* **69**, 2503 (1992); A.W. Snyder, L. Poladian, and D.J. Mitchell, *Opt. Lett.* **17**, 789 (1992).
- [24] P. Di Trapani *et al.*, *Phys. Rev. Lett.* **84**, 3843 (2000).
- [25] L. Torner and D.V. Petrov, *Electron. Lett.* **33**, 608 (1997); J.P. Torres, J.M. Soto-Crespo, L. Torner, and D.V. Petrov, *J. Opt. Soc. Am. B* **15**, 625 (1998).
- [26] W.J. Firth and D.V. Skryabin, *Phys. Rev. Lett.* **79**, 2450 (1997); D.V. Skryabin and W.J. Firth, *Phys. Rev. E* **58**, 3916 (1998).
- [27] D.V. Petrov *et al.*, *Opt. Lett.* **23**, 1444 (1998).
- [28] A.S. Desyatnikov and Yu.S. Kivshar, *Phys. Rev. Lett.* **87**, 033901 (2001).
- [29] Z.H. Musslimani, M. Soljačić, M. Segev, and D.N. Christodoulides, *Phys. Rev. E* **63**, 066608 (2001).
- [30] A. Desyatnikov, A. Maimistov, and B. Malomed, *Phys. Rev. E* **61**, 3107 (2000).
- [31] D. Mihalache, D. Mazilu, L.-C. Crasovan, B.A. Malomed, and F. Lederer, *Phys. Rev. E* **62**, R1505 (2000).
- [32] A.V. Buryak, Yu.S. Kivshar, and S. Trillo, *Opt. Lett.* **20**, 1961 (1995); M.A. Karpierz, *ibid.* **20**, 1677 (1995).
- [33] O. Bang, *J. Opt. Soc. Am. B* **14**, 51 (1997); O. Bang, Yu.S. Kivshar, and A.V. Buryak, *Opt. Lett.* **22**, 1680 (1997).
- [34] I. Towers, A.V. Buryak, R.A. Sammut, and B.A. Malomed, *Phys. Rev. E* **63**, 055601(R) (2001).
- [35] D. Mihalache, D. Mazilu, L.-C. Crasovan, I. Towers, B.A. Malomed, A.V. Buryak, L. Torner, and F. Lederer, *Phys. Rev. E* **66**, 016613 (2002).
- [36] I. Towers, A.V. Buryak, R.A. Sammut, B.A. Malomed, L.-C. Crasovan, and D. Mihalache, *Phys. Lett. A* **288**, 292 (2001); R.L. Pego and H.A. Warchall, *J. Nonlinear Sci.* **12**, 347 (2002).
- [37] B.A. Malomed, L.-C. Crasovan, and D. Mihalache, *Physica D* **161**, 187 (2002).
- [38] D. Mihalache, D. Mazilu, L.-C. Crasovan, I. Towers, A.V. Buryak, B.A. Malomed, L. Torner, J.P. Torres, and F. Lederer, *Phys. Rev. Lett.* **88**, 073902 (2002).
- [39] F. Smektala, C. Quemard, V. Couderc, and A. Barthélémy, *J. Non-Cryst. Solids* **274**, 232 (2000).
- [40] C. Zhan *et al.*, *J. Opt. Soc. Am. B* **19**, 369 (2002).
- [41] M. Quiroga-Teixeiro and H. Michinel, *J. Opt. Soc. Am. B* **14**, 2004 (1997).
- [42] V.I. Berezhiani, V. Skarka, and N.B. Aleksic, *Phys. Rev. E* **64**, 057601 (2001).
- [43] M.S. Bigelow, Q-Han Park, and R.W. Boyd, *Phys. Rev. E* **66**, 046631 (2002).
- [44] D. Mihalache, D. Mazilu, I. Towers, B.A. Malomed, and F. Lederer, *J. Opt. A: Pure Appl. Opt.* **4**, 615 (2002).
- [45] A.I. Maimistov, B.A. Malomed, and A. Desyatnikov, *Phys. Lett. A* **254**, 179 (1999).
- [46] J. Atai and B.A. Malomed, *Phys. Lett. A* **284**, 247 (2001).
- [47] H. Michinel *et al.*, *J. Opt. B: Quantum Semiclassical Opt.* **3**, 314 (2001).
- [48] T. Gisiger and M.B. Paranjape, *Phys. Rep.* **306**, 110 (1998).
- [49] J. Ruostekoski and J.R. Anglin, *Phys. Rev. Lett.* **86**, 3934 (2001).
- [50] D. Mihalache, D. Mazilu, L.-C. Crasovan, B.A. Malomed, and F. Lederer, *Phys. Rev. E* **61**, 7142 (2000).
- [51] Y.V. Kartashov, G. Molina-Terriza, and L. Torner, *J. Opt. Soc. Am. B* **19**, 2682 (2002); Y.V. Kartashov, L.-C. Crasovan, D. Mihalache, and L. Torner, *Phys. Rev. Lett.* **89**, 273902 (2002); L.-C. Crasovan, Y. V. Kartashov, D. Mihalache, L. Torner, Y. S. Kivshar, and V. M. Pérez-García, *Phys. Rev. E* **67**, 046610 (2003).
- [52] M. Soljačić, S. Sears, M. Segev, *Phys. Rev. Lett.* **81**, 4851 (1998); M. Soljačić and M. Segev, *Phys. Rev. E* **62**, 2810 (2000); *Phys. Rev. Lett.* **86**, 420 (2001).
- [53] A.S. Desyatnikov and Y.S. Kivshar, *Phys. Rev. Lett.* **88**, 053901 (2002).
- [54] A.G. Vladimirov, J.M. McSloy, D.V. Skryabin, and W.J. Firth, *Phys. Rev. E* **65**, 046606 (2002); D.V. Skryabin and A.G. Vladimirov, *Phys. Rev. Lett.* **89**, 044101 (2002).
- [55] H.S. Eisenberg, Y. Silberberg, R. Morandotti, A.R. Boyd, and J.S. Aitchison, *Phys. Rev. Lett.* **81**, 3383 (1998); R. Morandotti, U. Peschel, J.S. Aitchison, H.S. Eisenberg, and Y. Silberberg, *ibid.* **83**, 2726 (1999).
- [56] M.G. Vakhitov and A.A. Kolokolov, *Radiophys. Quantum Electron.* **16**, 783 (1973).
- [57] J.M. Soto-Crespo, D.R. Heatley, E.M. Wright, and N.N. Akhmediev, *Phys. Rev. A* **44**, 636 (1991); J. Atai, Y. Chen, and J.M. Soto-Crespo, *ibid.* **49**, R3170 (1994).
- [58] A. De Rossi, C. Conti, and S. Trillo, *Phys. Rev. Lett.* **81**, 85 (1998); D. Mihalache, D. Mazilu, and L. Torner, *ibid.* **81**, 4353 (1998).
- [59] J. M. Ortega and W. C. Rheinboldt, *Iterative Solution of Nonlinear Equations in Several Variables* (Academic Press, New York, 1970), p. 182.